Supplementary Information: Influence of membrane-cortex linkers on the extrusion of membrane tubes

This Supplementary Information provides additional details about the implementation of the membrane model and the influence of various simulation and experimental parameters on the mechanics of tube extrusion, and the experimental materials and procedures employed.

I. ADDITIONAL SIMULATION DETAILS

The membrane was modeled as a triangulated thin elastic sheet with hard sphere beads situated at every vertex. The system contains two types of beads, one type representing the membrane phospholipid patches and another corresponding to linker proteins. The dynamics of the system are evolved through a Monte Carlo scheme that involves two types of moves: vertex displacement moves and bond flip moves. The vertex displacement moves mimic the lateral diffusion of lipids and proteins, whilst also allowing for vertical membrane fluctuations. The bond flip moves ensure that the membrane preserves its fluidity by dynamically rearranging the connectivity (Fig. S1).

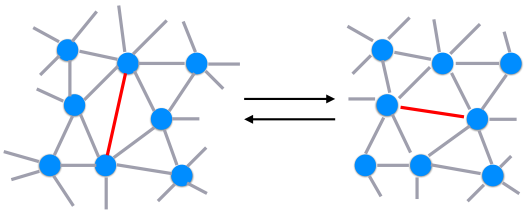

FIG. S1: **Bond flip move:** Monte Carlo moves are implemented to preserve the membrane's fluidity. The bond flips ensure that any bead will not have more than 6 neighbours at any time. These moves, together with the displacement moves, ensure that the lipids and proteins can diffuse freely in the membrane's plane.

II. SIMULATION RESULTS

A. Tube pulling force relaxation profile

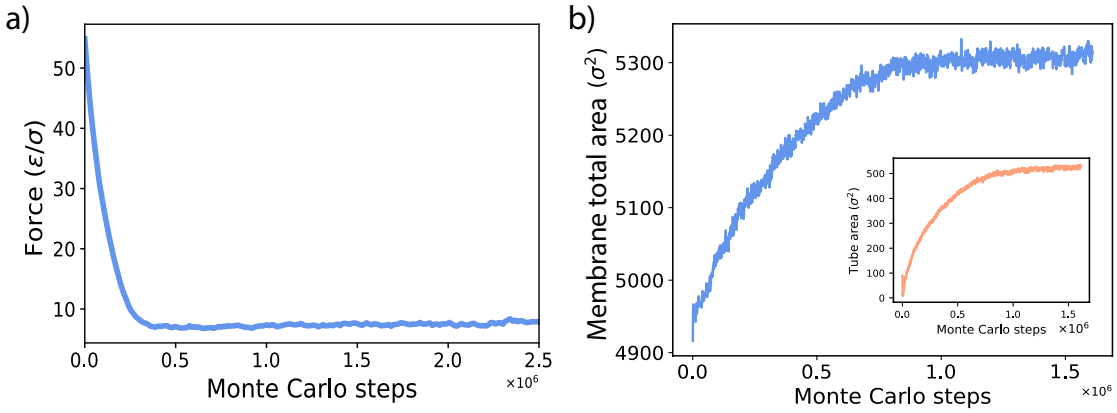

FIG. S2: **Force profile of a typical extrusion experiment.** a) The force acting on the protrusion's tip decays as the simulation proceeds, eventually converging at a non-zero value. b) The membrane area increases until it also reaches a steady state value (inset shows the tube area which follows a similar behaviour).

The point force acting on a protrusion's tip decreases until it reaches convergence at a non-zero value (Fig. S2a). The total membrane area and the tube area show a gradual increase until they stabilise at

a steady state value (Fig. S2b). The force cited in the main text is calculated from an average over one million Monte Carlo steps between 1 million and 2 million Monte Carlo steps. The force-extension curves were averaged over 5 different simulation seeds each, unless otherwise mentioned.

B. Influence of the linker proteins attachment energy on tube shape and composition

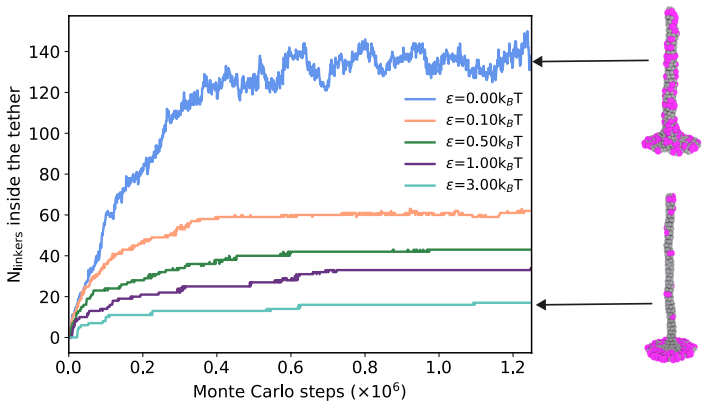

FIG. S3: **Number of linkers inside the tube for different attachment energies**. The flow of linkers inside the protein is heavily influenced by the protein binding. At higher attachment energies, the linkers will avoid the tube and partition preferentially in the membrane.

We next examined how the protein binding strength influences the tube shape and protein partitioning between the membrane and the tube. The linker attachment constant, k_{linker}, was varied between $\varepsilon = 0k_BT$ and $\varepsilon = 3k_BT$, whilst keeping the number density of proteins constant at 20%. At high linking attachment energies, the proteins partitioned preferentially into the membrane and avoided the tube entirely. This led to the formation of very thin elongated tubes with few proteins trapped inside (Fig. S3). At lower attachment energies, more linkers partitioned inside the tube, as the detachment cost is easier to overcome. The attachment energy highly influences the tube radius. The tube diameter decreases inversely proportional to the attachment energy (Fig. S4).

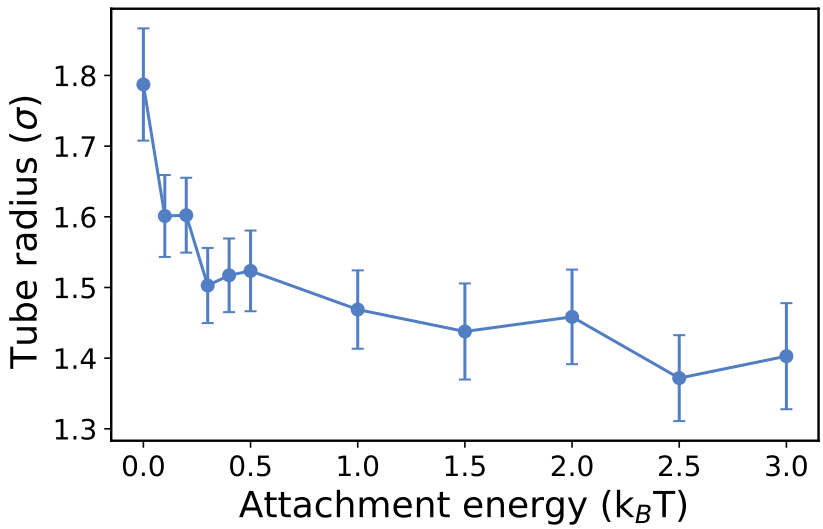

FIG. S4: **Influence of the attachment energy on tube radius**. The extruded tubes are thinner at higher attachment energies, as the proteins are pinned stronger to the membrane and hinder the free flow of lipid material inside the tube.

C. Distribution of linkers around the tube at different protein expression levels

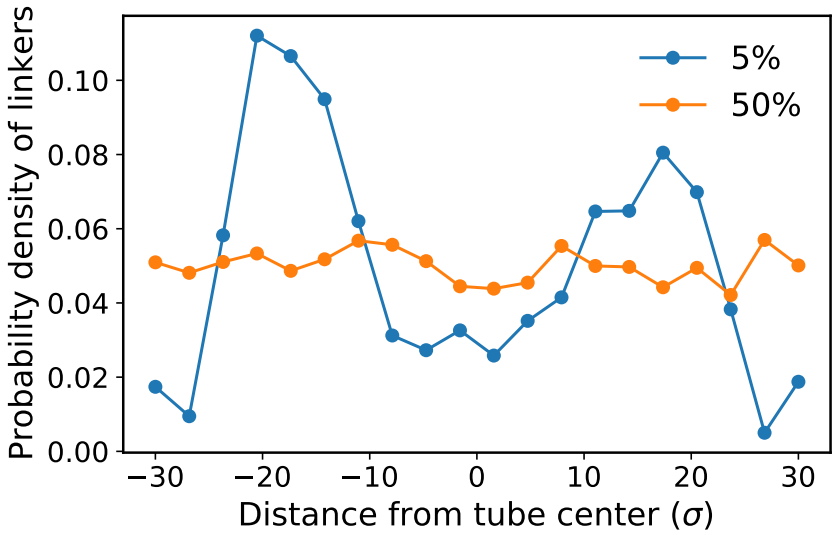

FIG. S5: **Probability density function of linkers on the membrane**. The probability density of linkers around the tube at 5% and 50% protein density.

The protein expression levels greatly influence the distribution profile of the linkers with respect to the tube. This, in turn, has an impact on the force measured in experiments. At low densities, the proteins reorganise around the tube and prefer segregating into protein rich areas (Fig. 3 of the main text and Fig. S5). In this regime, the protein levels do not significantly affect the force recorded in experiments (Fig. 2b). At higher densities, the proteins cannot avoid entering the tube as can be seen in Fig. S5. The linkers will be distributed uniformly across the entire membrane patch, with the tube's composition being identical to that of the membrane. The tube extrusion is thus energetically costly as it requires the detachment of the linkers from their rest positions. This leads to a dramatic increase in the measured force if the linkers are overexpressed.

D. Force-extension curve in the overexpression regime

The protein expression levels regulate the shape of the force-extension curve. At low protein densities, the shape of the curve is not significantly influenced by the protein density, showing a consistent characteristic force barrier followed by a flat plateau over a large extension (Fig. 2b of the main text). If the protein is overexpressed, the measured force increases dramatically as the proteins will be forced to detach from the membrane and they will be included in the tube (Fig. S6). The measured force will thus be significantly greater in this linker expression regime (as can also be observed from Fig. 2d of the main text).

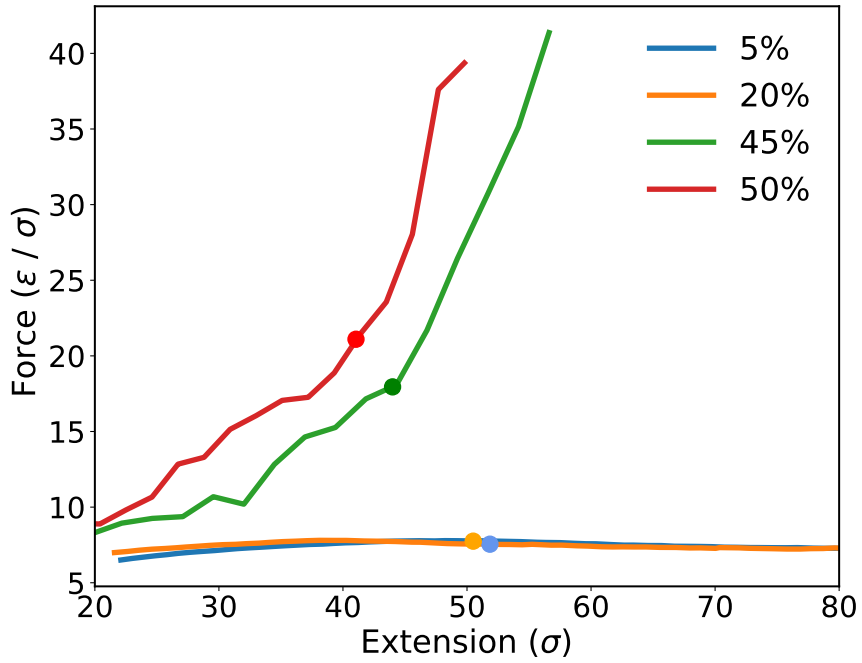

FIG. S6: **Force-extension curves at low and high linker densities**. At low densities, the force does not vary significantly over a wide range of tether extensions. The force increases substantially if the protein is overexpressed due to the high energetic cost associated with detaching the linkers from their rest positions. The markers correspond to the force and extension values recorded for a target extension of 60σ, as quoted in Fig. 2d of the main text.

III. EXPERIMENTAL RESULTS

A. Tether force convergence

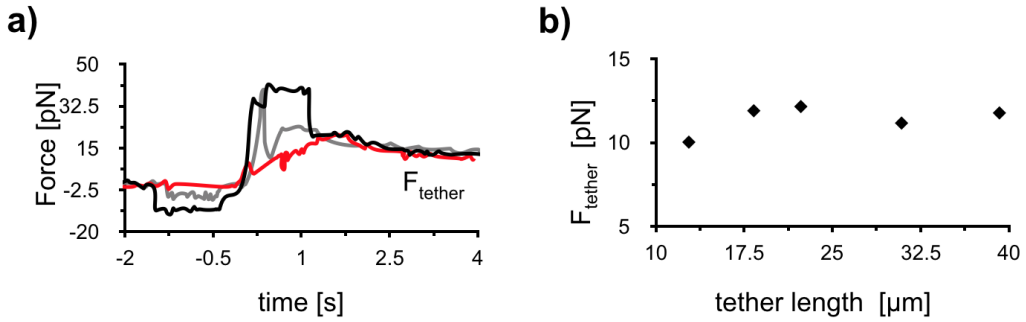

FIG. S7: **Tether forces rapidly converge to $\mathbf{F}_{\text{tether}}$ and are independent of the tether length.** a) Full force profile corresponding to three membrane tethers pulled from different cells during one experiment. While the initial force profile is very different for each of the cells since its depends on the contact area between the bead and the cell membrane, individual tether holding forces converge to similar values within seconds. b) Tether holding force of an individual membrane tether as a function of tether length.

B. Tube pulling force for different cell types

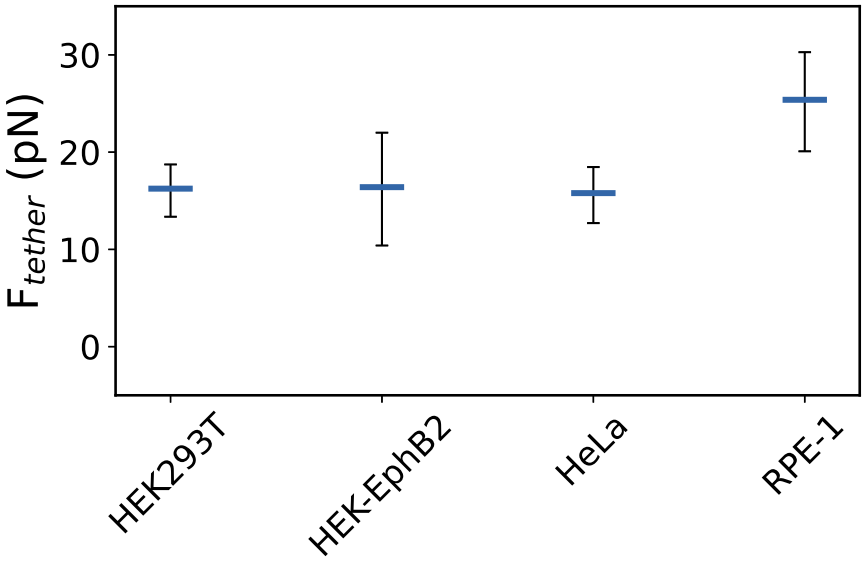

FIG. S8: **Static tether forces depend on cell type.** Tether forces in HEK293T (n=5), HEK-EphB2 (n=16), HeLa (n=5) and RPE-1 (n=5) cells.

C. Expression levels of proteins analyzed by western blot and immunofluorescence

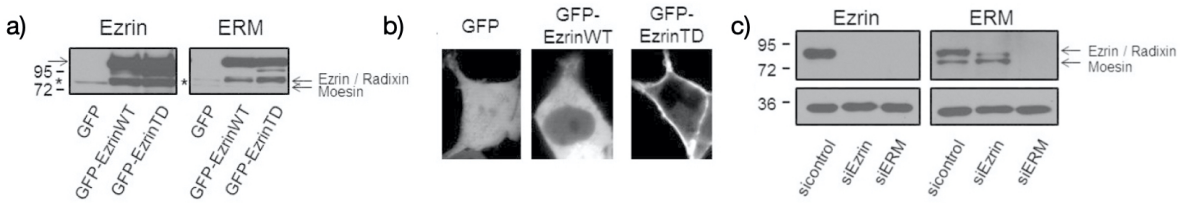

FIG. S9: **Expression levels of proteins analyzed by western blot and immunofluorescence.** (a) Western Blots showing expression levels of proteins after expressing GFP labeled constructs in HEK293T cells. Expression level of GFP-Ezrin is superior to the endogenous ezrin (*) and ERM. (b) Representative equatorial plane fluorescence images of HEK293T cells expressing fluorescent recombinant proteins. Note that we selected cells with similar expression levels of fluorescent proteins. GFP-EzrinWT is detected in the cytoplasm and at the plasma membrane and GFP-EzrinTD is predominantly at the plasma membrane. (c) Western blots showing expression levels of proteins after depletion using siRNA, detected with antibodies against Ezrin and ERM, respectively. All siRNA treatments reduce the protein levels below detection levels. GAPDH is the loading control. Note that Ezrin and Radixin are not well separated and correspond to one band (upper band) when detected with anti-ERM antibodies. Thus this band seems slightly shifted and only partially reduced in cells treated by siEzrin. The 3 ERM are fully depleted with siERM.

D. Fitting of relaxation curves

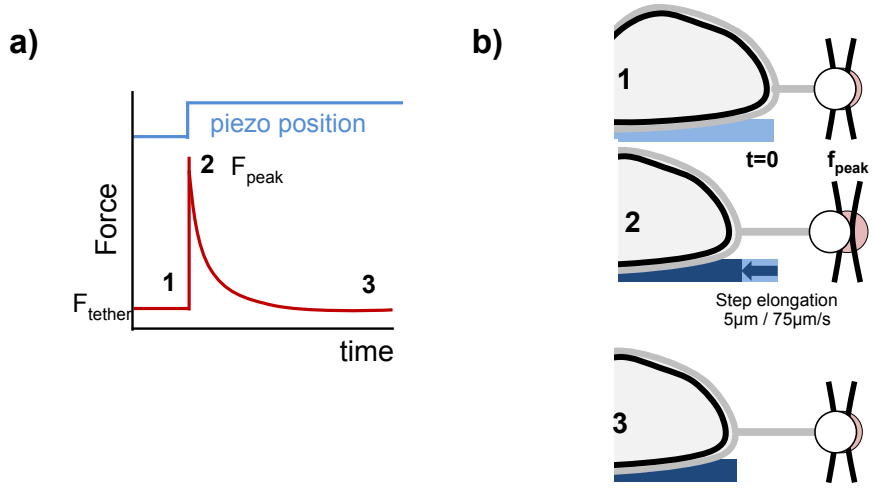

FIG. S10: **Step elongation of existing membrane tethers to assess tether relaxation.** a) Three force regimes can be observed during step elongation of an existing membrane tether. b) A relaxed membrane tether with holding force F_{tether} (1) is elongated by imposing a fast step displacement of a piezo-controlled stage leading to a peak in force (2). Over time the force relaxes back to the initial value of the tether force (F_{tether}).

A 5 μm extension at 75 μm/s was applied on a preformed tube held at a static tether force F_{tether} (Fig. S10). During elongation we observed a rise up to a peak force F_{peak} when elongation is stopped, defined as $t = 0$. We measured the force relaxation over time $F(t)$ at constant tether length in the presence or in the absence of ERM (Fig. 5b of the main text). Early work on tether pulling from cells generally considered a single exponential relaxation for the force [1–3]. Recent work both on vesicles with a reconstituted actin cortex and cellular membranes vesicles revealed that the force relaxation cannot satisfyingly be described with a single exponential, but rather contains both a fast exponential decay (on the order of seconds) independent of actin and a linear slow decay that depend on actin and appears diffusive [4]. We confirmed that a single exponential decay does not account properly for our data. In contrast, our data is correctly described by a simple model of a composition gradient across the neck: the tension gradient, reflected by the tether force, is dissipated with a characteristic relaxation time that depends on membrane-component diffusion and thus possibly on the density of actin-PM linkers that form 'obstacles', thus reducing their diffusion. We have fitted the force relaxation data (Fig. 5b of the main text) with:

$$F(t) = \sqrt{F_{\text{peak}}^2 - (F_{\text{peak}}^2 - F_0^2) g(t/\tau)} \tag{S1}$$

where:

$$g(t/\tau) = 1 - e^{-(t/\tau)}(\text{erf}(c\sqrt{t/\tau})) \tag{S2}$$

with the relaxation time τ as the only free parameter. τ is expected to depend on the diffusion of the minority component in the cell membrane, which in turn is expected to be influenced by the density of linkers at the interface between plasma membrane. Our data set fits well with equation S1 (Fig. 5b). As expected, the relaxation time is reduced when ERM are depleted (0.7 s in the control and 0.3 s after ERM depletion, Fig. 5b).

IV. MATERIALS & METHODS

Cell culture. HEK293T, HEK-EphB2 [5], HeLa, RPE-1 and NIH3T3 cells were cultured at 37°C and 5% CO2 in DMEM GlutaMAX medium (gibco 61965-026), supplemented with 10% fetal bovine

serum (gibco 10270106), and 1% Penicillin Streptomycin (gibco 15070063).

Plasmids
Carboxy-terminally-tagged GFP-EzrinWT and and GFP-EzrinTD [6, 7] fusion protein were previously described.

siRNA. siEzrin (L-017370-00), ERM triple depletion as described in [8] with siEzrin (EZR J-017370-08), siRadixin (RDX J-011762-07), siMoesin (MSN J-011732-08), and non-targeting control siRNA (D-001810-10), all from Dharmacon.

Transfection. Transfection of cells with protein-encoding plasmids was performed using Lipofectamine^{TM} 2000 (Invitrogen 11668-019). 250,000 cells per well were seeded in a 6 well plate (TPP 92006) 24 hours prior transfection with 1 μg of the other plasmids, per well. The transfection mix was prepared as follows: 5 μL of Lipofectamine^{TM} 2000 and the respective amount of DNA were added to 250 μL of OptiMEM (gibco 31985-062) each in a separate 2 mL microtube (Sarstedt 72.695.500). After 5 minutes of incubation at room temperature, both solutions were united and mixed by pipetting up and down several times and left to incubate at room temperature for 15 minutes. The resulting 500 μL of transfection mix was added to the corresponding well, containing 1.5 mL freshly added, pre-warmed full medium. The medium was exchanged for full medium 6-8 hours after transfection and cells were assessed after $\sim$24h of transfection.

Cells were transfected with siRNA using Lipofectamine^{TM} RNAiMAX (Invitrogen 13778-030). The transfection mix was prepared as follows: 5 μL of Lipofectamine^{TM} RNAiMAX and the respective amount of siRNA were added to 250 μL of OptiMEM (gibco 31985-062) each in a separate 2 mL microtube (Sarstedt 72.695.500). After 5 minutes of incubation at room temperature, both solutions were united and mixed by pipetting up and down several times and left to incubate at room temperature for 30 minutes. The resulting 500 μL of transfection mix was added to the corresponding well, containing 1.5 mL freshly added, pre-warmed full medium.

For depletion of Ezrin, ERM, and respective controls, 80,000 cells were seeded out 24h prior treatment and transfected twice, the secondary transfection following 48 hours after the first. Cells were assessed after a total of $\sim$96 hours. The respective concentrations of siRNA were 20 nM for Ezrin, and 10 nM for each siRNA of Ezrin, Radixin, and Moesin, thus yielding a total of 30 nM for ERM depletion.

Western blots. After washing with PBS cells were lysed in 1.5x SDS-loading buffer supplemented with β-mercapto-ethanol pre-heated to 95°C. After treatment with (Sigma),benzonase cell lysates were analyzed by SDS-PAGE and transferred to nitrocellulose membranes. Ezrin and ERM were detected with antibodies indicated on the figures.

Experimental chamber. Cells were grown on 25 mm circular glass cover slips (VWR ECN 631-1584) prepared in the following way: 1) Cleaning with Isopropanol, Ethanol, water, Ethanol and then dried under a cell culture hood. 2) Coating with a 20 μg/mL solution of Laminin (Sigma L2020) for $\sim$2 hours at 37°C. Cells were analyzed 16-20 hours after seeding out 250000 cells per glass coverslip. The medium was exchanged for CO2-independent DMEM medium (gibco 21063-029), supplemented with 1.5 mg/mL β-Casein (Sigma C6905) to passivate the surface (experiment medium), 1 hour before a measurement. The glass cover slips were fixed on a custom-made experimental chamber using vacuum grease (Sigma Z273554). The cells were maintained in experimental medium throughout the experiment supplemented with carboxylated polystyrene beads (Spherotech CP-30-10, 3.07 μm nominal diameter, 0.001 % suspension) used for tether pulling. The temperature was maintained at $\sim$37°C throughout the experiment using a custom-built objective-heater based on a resistive collar.

Fluorescence images. Transfected cells were imaged using a conventional confocal microscope at the equatorial plane to assess expression and localization of fluorescently tagged proteins prior to tube pulling.

Optical Tweezer. The custom-built optical tweezer set-up consisted of a 1064 nm Ytterbium fiber laser (IPG Photonics) and a Nikon C1 Plus confocal microscope. We employed a Nikon CFI Plan Fluor 100x, NA 1.3 oil immersion objective which was surrounded by a resistive collar to allow heating of the objective to maintain a stable temperature of 37°C within the experimental chamber. The sample chamber was fixed on a voltage-controlled piezo-drive (MadCityLabs Nano-LP100). Bright field images of the bead were acquired using an EM-CCD camera at a frame rate of $\sim$180 frames per

second (iXon DU-897, Andor), and analyzed by a custom MATLAB script. Forces were calculated from bead positions following the equation: $F = k(x - x_0)$, where k is the trap stiffness, x the position of the bead, and x_0 the reference position at equilibrium. Trap stiffness calibration was obtained using the viscous drag method, including Faxen's correction for calibration close to surfaces [9], with a trap stiffness adjusted to 44 pN/μm at 3W input power (400mW at the back focal plane of the objective).

Tube pulling. Using a custom LabVIEW program to control the piezo stage, tubes were pulled, by trapping an isolated floating bead, bringing it into contact with the cell for a short period ($\sim$3 seconds), and then moving the cell away from the trap center in x direction using the piezo. For measuring the static tether force, the tube was about 10μm long and held steady for at least 10 seconds. For the dynamical force measurements, the initial tether had a length of about 10μm. While the initial force overshoot for tether formation varied widely, a relaxation of the force to a stable plateau could generally be observed within the first 10 seconds after tube formation.

Step elongation. Once the tether holding force was stabilized, step elongation of the tube was performed by imposing a step-displacement of the piezo stage away from the trap center of 5 μm at a speed of 75 μm/s. The force relaxation was then recorded.

The change in force is monitored by imaging the bead holding the tube at high temporal resolution (175 fps). This allows following the peak in force upon step elongation and the subsequent relaxation.

Statistics. Data sets for effective membrane tension and relaxation timescale were analyzed by one-way ANOVA. If the null hypothesis was successfully rejected, F-tests were conducted on a paired basis to compare variances and, depending on the outcome, two-tailed t-tests assuming equal or unequal variances were employed. Only p-values smaller than 0.05 are displayed in the figures.

[1] William C Hwang and Richard E Waugh. Energy of dissociation of lipid bilayer from the membrane skeleton of red blood cells. *Biophysical Journal*, 72(6):2669, 1997.

[2] Liselotte Jauffred, Thomas Hønger Callisen, and Lene Broeng Oddershede. Visco-elastic membrane tethers extracted from escherichia coli by optical tweezers. *Biophysical journal*, 93(11):4068–4075, 2007.

[3] Zhiwei Li, Bahman Anvari, Masayoshi Takashima, Peter Brecht, Jorge H Torres, and William E Brownell. Membrane tether formation from outer hair cells with optical tweezers. *Biophysical journal*, 82(3):1386–1395, 2002.

[4] Clément Campillo, Pierre Sens, Darius Köster, Léa-Laetitia Pontani, Daniel Lévy, Patricia Bassereau, Pierre Nassoy, and Cécile Sykes. Unexpected membrane dynamics unveiled by membrane nanotube extrusion. *Biophysical journal*, 104(6):1248–1256, 2013.

[5] Marie-Thérèse Prospéri, Priscilla Lépine, Florent Dingli, Perrine Paul-Gilloteaux, René Martin, Damarys Loew, Hans-Joachim Knölker, and Evelyne Coudrier. Myosin 1b functions as an effector of ephb signaling to control cell repulsion. *Journal of Cell Biology*, 210(2):347–361, 2015.

[6] Richard F Lamb, Bradford W Ozanne, Christian Roy, Lynn McGarry, Christopher Stipp, Paul Mangeat, and Daniel G Jay. Essential functions of ezrin in maintenance of cell shape and lamellipodial extension in normal and transformed fibroblasts. *Current Biology*, 7(9):682–688, 1997.

[7] Sylvie Coscoy, François Waharte, Alexis Gautreau, Marianne Martin, Daniel Louvard, Paul Mangeat, Monique Arpin, and François Amblard. Molecular analysis of microscopic ezrin dynamics by two-photon frap. *Proceedings of the National Academy of Sciences*, 99(20):12813–12818, 2002.

[8] Dafne Chirivino, Laurence Del Maestro, Etienne Formstecher, Philippe Hupé, Graça Raposo, Daniel Louvard, and Monique Arpin. The erm proteins interact with the hops complex to regulate the maturation of endosomes. *Molecular biology of the cell*, 22(3):375–385, 2011.

[9] Keir C Neuman and Steven M Block. Optical trapping. *Review of scientific instruments*, 75(9):2787–2809, 2004.